

Symmetry Completion Test: A Novel Approach for Visual Distortion Mapping and Correction Using Symmetry Constraints

Ye Ling¹^a, David M. Frohlich²^b, Tom H. Williamson³^c and Jean-Yves Guillemaut¹^d

¹Centre for Vision, Speech and Signal Processing, University of Surrey, Guildford, U.K.

²Digital World Research Centre, University of Surrey, Guildford, U.K.

³Guy's and St Thomas' NHS Foundation Trust, London, U.K.

Keywords: Metamorphopsia, Visual Distortion, Image Warping, Assistive Technology.

Abstract: Metamorphopsia, commonly referred to as distorted vision, is a serious visual impairment which remains uncorrectable by optical glasses or contact lenses. This paper presents a novel approach to digitally map visual distortion based on patient feedback. The approach is based on the use of low-level geometrical constraints (central symmetry) which provide a simple and intuitive mechanism for a patient to provide feedback on their perceived visual distortion. We derive a set of fundamental constraints and show how visual distortion mapping can be framed as an optimisation problem. Critically, a parametric distortion model based on MLS is used to reduce the dimensionality of the problem and enable detailed visual distortion estimation. An extensive evaluation using simulated data demonstrates the accuracy and robustness of the approach. This approach opens up the possibility of correcting for visual distortion by applying the inverse mapping on the input stream to for instance VR see-through devices or screen-based devices.

1 INTRODUCTION

Vision constitutes a vital sensory function facilitating the human body's perception of the external environment. The World Health Organization (WHO) reports that the global population afflicted with visual impairment approaches approximately 2.2 billion individuals (WHO-Newsroom, 2023). Common conditions such as myopia and presbyopia can be corrected through the utilization of optical glasses or contact lenses. However, there are numerous other visual impairments that are not amenable to correction, thereby necessitating the use of low-vision aids, which are only partially effective for a subset of these impairments. Examples of such aids include large print books, handheld magnifiers, CCTV screen magnifiers, microscope and telescope devices, tinted sunglasses and filters, and assistive settings on screens that enable modifications to font size, contrast and colour. The possibility of incorporating some of these functions into head-mounted displays

has been explored experimentally, on and off, for over 20 years (Massof, 1998). In recent years, there has been a growing commercial viability of such systems, leading to the emergence of various low vision "see-through" headsets in the market, such as eSight Eyewear, NuEyes Pro Smart Glasses and IrisVision (Deemer et al., 2018). Most of these devices typically incorporate basic manual adjustments for magnification, contrast, and colour settings, and in some cases, they may also feature text recognition capabilities for speech output. These show some benefit to low vision sufferers, but a challenge now exists to extend the functionality of these headsets to more complex conditions and customize them to the unique capabilities of individuals (Zhao et al., 2019), such as metamorphopsia. This paper introduces a new approach for the mapping and correction of metamorphopsia or distorted vision, which is a common symptom of age-related macular degeneration and other retinal disorders.

Metamorphopsia, a condition characterized by visual distortion, results in the perception of straight lines as curved, as depicted in Figure 1. Figure 1a shows the well-known painting "Mona Lisa". However, from the perspective of an individual suffering from metamorphopsia, some regions are perceived as

^a <https://orcid.org/0000-0002-9973-2302>

^b <https://orcid.org/0000-0003-3483-9915>

^c <https://orcid.org/0000-0002-1879-449X>

^d <https://orcid.org/0000-0001-8223-5505>

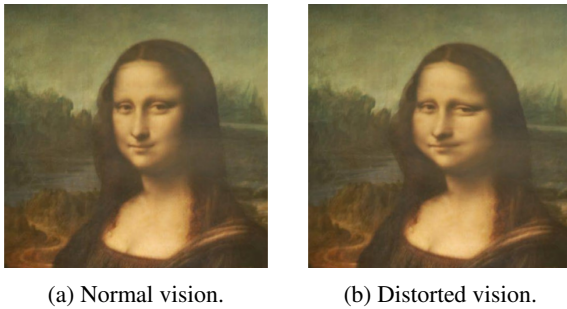


Figure 1: Illustration of the effects of metamorphopsia. An image seen by a healthy person (a) will appear distorted (b) to a person suffering from metamorphopsia.

distorted. Figure 1b shows a simulated representation of this perceived distorted vision. According to previous studies (Bouwens and van Meurs, 2003; Bex, 2010; Burke, 1999; Cohen et al., 2003; Jensen and Larsen, 1998; Mansouri et al., 2009; Zur and Ullman, 2003; Ugarte et al., 2013; Simunovic, 2015), this issue is considered to be caused by the displacement of photoreceptors or the re-organization of visual cortex and perception adjustment after sensory input interruption from the retina in macular disease. Traditional optical correction methods involving glasses and contact lenses fail to adequately address these distortions since they primarily stem from retinal damage rather than a mere obstruction of light passage through the eye. It also moves with the eye, making fixed optical correction useless. Regrettably, no effective clinical treatment method for this problem has been identified.

Digital approaches open up novel avenues to overcome those limitations by manipulating the image presented to the user with a view to restoring healthy vision. The advancement of Augmented Reality (AR) headsets and 3D displays serves as a solid hardware foundation to support these efforts. The fundamental concept underlying the utilization of digital technologies involves the application of inverted deformations within the video stream transmitted through see-through devices, thereby enabling the compensation of visual distortions experienced by the affected eye. Thus, the estimation of the visual distortion mapping becomes the major task.

This paper proposes a monocular approach for accurate mapping of visual distortion termed the ‘‘Symmetry Completion Test’’. Being monocular, the approach can be applied separately to each eye and it does not rely on having a distortion-free reference eye to guide the distortion mapping process. The key idea behind the approach is to leverage simple low-level geometric constraints (central symmetry) in order to interactively discover the distortion experi-

enced by a patient. A distortion model based on Moving Least Squares (MLS) is also introduced in order to parametrise distortion using a small number of variables. Patient feedback on each symmetry constraint is used to formulate an energy function which is optimised to retrieve the model parameters representing the visual distortion experienced by each participant.

The paper makes the following key contributions. First, it introduces the central symmetry constraints that form the foundation for the distortion mapping test. These are rigorously developed with full mathematical detail and derivation provided. Second, we demonstrate how these can be incorporated into an effective optimisation framework to retrieve visual distortion. In particular, we show how a low-dimensional parametric model can be leveraged to overcome the high-dimensionality issues pertaining to estimating visual distortion across the visual field. Finally, we carry out an extensive evaluation to validate the approach.

The remainder of this paper is organized as follows. Section 2 gives an overview of the literature relevant to this study, highlighting the existing body of knowledge in the field. Section 3 introduces the methodology and implementation details. Section 4 presents the results obtained from the simulation experiments. Section 5 concludes by summarising the findings and discussing avenues for future work.

2 RELATED WORK

The idea of utilizing computer vision technology to improve impaired human vision can be traced back to the 80s. (Peli and Peli, 1984) introduced an application that employed adaptive image enhancement techniques to enhance visual perception in individuals with low vision. Additionally, enlargement techniques have gained significant popularity in the realm of low vision improvement, as evidenced by studies (Vargas-Martín et al., 2005; Szpiro et al., 2016; Zhao et al., 2019). Colour inversion is a useful method for low-vision people. (Szpiro et al., 2016) introduces a method for low vision improvement by inverting colours while (Peli, 1994) uses white and black to present text. Both of them achieve the purpose of improving low vision by using high contrast. In addition, edge detection emerges as another viable method for enhancing visual acuity in individuals with low vision, as exemplified by studies (Vargas-Martín et al., 2005; Szpiro et al., 2016; Zhao et al., 2019). While these above methods have proven effective in addressing various visual impairments, they fall short in their ability to correct metamorphopsia. As described in

Section 1, metamorphopsia presents unique and unpredictable visual distortions. Consequently, correcting metamorphopsia proves to be a formidable challenge in the absence of an accurate mapping of the specific visual distortions associated with this condition.

The methodology known as square completion task, as introduced in (Wiecek et al., 2015), presents an approach to map the visual distortion. This method involves presenting four corner points and a central fixation point to the participant. Among the four corners, one serves as a reference point, while the participant's task is to adjust the positions of the remaining three corners until they form a regular square within their visual field. Subsequently, the participant is required to confirm a midpoint on each side of the square. Consequently, data for eight points can be obtained based on a single corner of the square. This process is repeated with different reference points until all four corners have been tested. Ultimately, the mean value of the eight points obtained from each corner is employed to describe the participant's visual distortion. Although it attempts to quantify the distortion, this approach suffers from two key limitations. Firstly, it only provides a sparse characterisation of the distortion pattern, being limited to 8 points within the field of view. This restricted sampling may fail to capture the full extent and complexity of the visual distortion. Secondly, the use of averaging to fuse the results from the different trials may introduce errors when confronted with asymmetric distortions.

A useful method for mapping and compensating for distorted vision is presented in (Bozzelli et al., 2020; Cimmino et al., 2021). In this approach, participants are tasked with adjusting a generated Amsler grid by manipulating the positions of its vertices until the grid assumes the appearance of a regular, straight-line grid. Subsequently, the developed application utilizes this mapping of geometrical deformation to correct visual distortion in real-time through the manipulation of the video stream in an AR headset. However, this method is not without its limitations. Many participants reported discomfort while wearing the AR headset during the operation, which adversely affected their overall experience. Additionally, the calibration procedure required for accurate mapping was found to be time-consuming, further impeding the efficiency of the process. Consequently, a mere 28% of participants successfully completed the entire testing procedure, indicating the need for further improvement in terms of comfort and usability to enhance user participation and compliance.

The interactive line manipulation method represents an innovative approach aimed at visualizing

the distorted view experienced by individuals with metamorphopsia (Ichige et al., 2019; Moritake et al., 2021; Zhu et al., 2022). This technique detects distortion through the analysis of horizontal and vertical straight lines and subsequently corrects the distortion by adjusting the parameters associated with the anchor points within the affected area. By applying the derived deformation to an input image, a compensatory effect on the visual distortion can be achieved. However, one notable challenge encountered in the implementation of this method is the uncontrollable duration of the testing process. Particularly in cases where the distortion exhibits complexities, the experiment duration tends to be significantly prolonged. This issue poses practical limitations, as it hampers the efficiency and feasibility of the technique, necessitating further exploration and refinement to expedite the testing procedure without compromising the accuracy of the distortion analysis and correction.

Another interesting approach is the one introduced by (Zaman et al., 2020; Ong et al., 2022). Different from the methods introduced before, the mapping of visual distortion is obtained first and then the purpose of correcting the visual distortion is achieved by applying the mapping. In this study, a novel approach is introduced, wherein the distorted areas are substituted with black holes of equivalent size. Thus, the deformation is suppressed by integration with the normal vision of the healthy eye. The overall deformation is effectively mitigated. While this particular method may not directly map or correct the visual deformation, it offers an interesting means of alleviating distorted vision. The incorporation of black holes to replace the affected areas holds promise in reducing the visual impact of the distortion by leveraging the integration of the remaining intact visual information. Although further research is necessary to fully evaluate and optimize the effectiveness of this approach, it represents a noteworthy avenue for mitigating the effects of distorted vision.

None of these previous tests have yet demonstrated suitability for extensive clinical implementation. This paper aims to address some of the previous shortcomings by introducing a novel and practical approach that enables accurate dense visual distortion mapping. A key insight is the combination of the use of low-level geometric constraints (central symmetry constraints), that provide a simple way for the patient to provide constraints on distortion, with the use of a low-dimensional parametric model of visual distortion, to achieve dense and scalable mapping. An initial demonstration of the test was presented in (Ling et al., 2023).

3 METHODOLOGY

This section describes the proposed approach for monocular mapping of visual distortion from low-level geometric constraints provided by the user. The section starts by formulating the problem in mathematical terms and stating the assumptions. It then introduces the proposed geometric constraints underpinning the approach. Next, it describes how visual distortion is inferred from these by framing the problem as an energy minimisation problem and introducing some regularisation constraints. Finally, the implementation details are provided.

3.1 Problem Statement and Assumptions

Consider the problem of recovering a 2D deformation field \mathbf{d} defined over the visual field I of a patient's eye affected by metamorphopsia. \mathbf{d} represents the perceived distortion as a 2D displacement vector at each point in I . Note that \mathbf{d} models visual distortion only in a single eye. However, the approach is easily extended to model binocular metamorphopsia by recovering a separate displacement field for each eye. Without loss of generality, we describe the recovery of the deformation field for a single eye in the rest of the paper.

Given that the visual distortion manifests itself as a result of retinal issues (e.g. detached retina), it tracks the gaze direction of the patient. Visual distortion is therefore mapped in the visual field centred around the gaze direction of the patient. To eliminate the dependency on gaze direction, the patient is requested to rest their head on a chin-rest and maintain their focus on a fixation point located at the centre of the screen throughout the test. This assumption may be relaxed in the future through the use of eye-tracking technology.

3.2 Central Symmetry Constraints

The patient's distortion is not directly observable. The main idea behind the proposed approach is to derive a constraint on the visual distortion through the completion of a simple interactive test involving low-level geometric constraints, more specifically central symmetry. While other types of low-level constraints may be considered (e.g. axial symmetry, collinearity or orthogonality), central symmetry was selected for the intuitiveness of the resulting test.

In a nutshell, the patient is presented with three points on a screen such that one of them is the midpoint of the segment defined by the other two. These

points would be perceived as satisfying a central symmetry constraint by a person with healthy vision, but will usually not satisfy this constraint for a patient suffering from metamorphopsia if the points fall within the area of the visual field affected by visual distortion. The patient is therefore asked to displace one of the points to satisfy central symmetry. Such a test provides a constraint, which can be used to infer the deformation field. Next, we provide a derivation of the two types of symmetry constraints considered depending on which point is manipulated.

3.2.1 Type 1 Constraint: Side Point Correction

Let us consider three points P , O and Q such that O is the midpoint of the segment PQ . We also assume O is located at the centre of the screen and used as a fixation point. Since P , O and Q satisfy the central symmetry constraint in screen coordinates, as shown in Figure 2a, we have:

$$2O = P + Q. \quad (1)$$

However, as a result of visual distortion displayed in Figure 2b, the patient will perceive the points as distorted with the following locations in the patient's view:

$$P_d = P + \mathbf{d}(P), O_d = O + \mathbf{d}(O), Q_d = Q + \mathbf{d}(Q). \quad (2)$$

These will not normally satisfy the symmetry constraint.

The patient is required to displace the side point Q to satisfy the central symmetry constraint, as shown in Figure 2c. Let us denote by $\mathbf{v}_P(Q)$ the 2D displacement that needs to be applied to Q in order to satisfy that constraint and by $Q' = Q + \mathbf{v}_P(Q)$ the resulting displaced point in screen coordinates. Due to visual distortion, Q' will be perceived at the following location in the patient's view:

$$Q'_d = Q' + \mathbf{d}(Q') = Q + \mathbf{v}_P(Q) + \mathbf{d}(Q'). \quad (3)$$

The perceived points P_d , O_d and Q'_d now satisfy the central symmetry constraint in the patient's view:

$$2O_d = P_d + Q'_d. \quad (4)$$

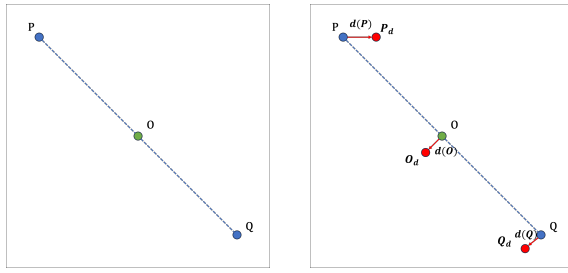
Substituting (2) and (3) into (4), we obtain:

$$2O + 2\mathbf{d}(O) = P + \mathbf{d}(P) + Q + \mathbf{v}_P(Q) + \mathbf{d}(Q'), \quad (5)$$

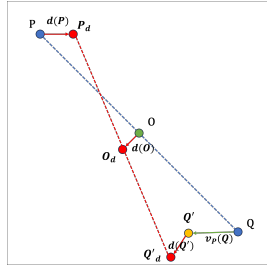
which, after simplification using (1) and rearranging, gives:

$$\mathbf{d}(P) + \mathbf{d}(Q') - 2\mathbf{d}(O) + \mathbf{v}_P(Q) = \mathbf{0}. \quad (6)$$

(6) defines a constraint relating the correction made to the side point Q by the user to enforce central symmetry and the visual distortion at P , O and Q' .



(a) Normal vision. (b) Distorted vision.



(c) Constraint diagram.

Figure 2: Illustration of the Type 1 symmetry constraint.

3.2.2 Type 2 Constraint: Central Point Correction

Let us consider again three points P , O and Q , but this time such that the user-controlled point Q is the midpoint of the segment OP . The diagram used to explain the relationship can be found in Figure 3. As in the previous case, we assume O is located at the centre of the screen and used as a fixation point. The derivation of the resulting constraint is similar to that of the previous constraint and we therefore only describe the main steps for brevity, reusing the same notation. It follows from the symmetry constraint that:

$$2Q = P + O. \quad (7)$$

After the displacement of Q by the patient, the perceived points P_d , O_d and Q'_d satisfy the central symmetry constraint in the patient's view:

$$2Q'_d = P_d + O_d. \quad (8)$$

Substituting (2) and (3) into (8), we have:

$$2Q + 2v_P(Q) + 2d(Q') = P + d(P) + O + d(O), \quad (9)$$

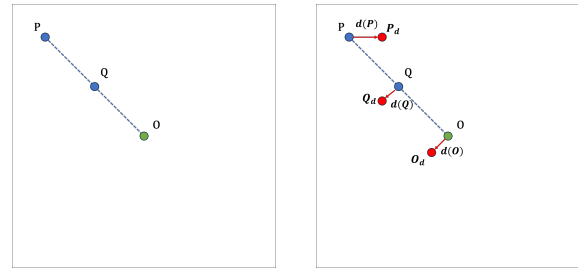
which can be simplified using (7) and rearranged to:

$$2v_P(Q) + 2d(Q') - d(P) - d(O) = 0. \quad (10)$$

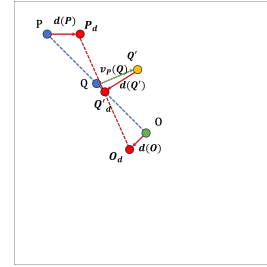
(10) defines a constraint relating the correction made to the central point Q by the user to enforce symmetry and the visual distortion at P , O and Q' .

3.3 Cost Function Definition and Optimisation

Recovery of the visual distortion d from the previous constraints is framed as an energy minimisation



(a) Normal vision. (b) Distorted vision.



(c) Constraint diagram.

Figure 3: Illustration of the Type 2 symmetry constraint.

problem. We consider multiple symmetry constraints of both types introduced earlier and obtained by considering different point locations to sample the visual field. In our implementation, we consider 24 reference points arranged in a 5×5 regular grid covering 8° as described in Figure 4. The reference point defines the location of P for each of the two types of constraint.

(6) and (10) each define two constraints on the visual distortion d (one for each axis). However, each symmetry constraint generates four unknowns relating to the displacements at P and Q' (two unknowns per point). As such, this defines an under-constrained system of equations and direct optimisation is not possible. To overcome this, we introduce some regularisation by using a parametric model to represent the visual distortion d . More specifically, the Moving Least Squares (MLS) introduced in (Schaefer et al., 2006) is used to parametrise distortion using a small number of control points. In our implementation, eight control points are used. These include four movable handles used to control the image deformation and four fixed corner points used to anchor the image. This defines a total of eight degrees of freedom (two per movable handle). The corner point constraints embedded in our MLS model are useful to resolve the rigid image transformation ambiguity (rotation, translation, scaling) present in the cost function.

The solution is found by finding the visual distortion d which minimises the following energy func-

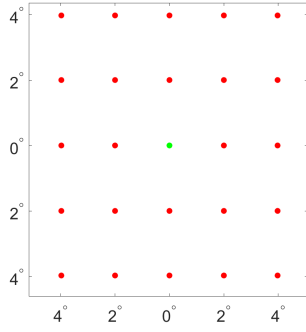


Figure 4: Reference points distribution within the visual field. The red points denote the reference points, while the green point denotes the fixation point.

tion:

$$E(\mathbf{d}) = \sum_{i=0}^{N_1} L_{\delta_1}(e_1(\mathbf{d}, i)) + \sum_{i=0}^{N_2} L_{\delta_2}(e_2(\mathbf{d}, i)), \quad (11)$$

where N_1 and N_2 denote the number of Type 1 and Type 2 symmetry constraints respectively. The individual errors for each type of constraint are derived from (6) and (10) and defined as follows:

$$e_1(\mathbf{d}, i) = \|\mathbf{d}(\mathbf{P}_i) + \mathbf{d}(\mathbf{Q}'_i) - 2\mathbf{d}(\mathbf{O}) + \mathbf{v}_{\mathbf{P}_i}(\mathbf{Q}_i)\|, \quad (12)$$

$$e_2(\mathbf{d}, i) = \|2\mathbf{v}_{\mathbf{P}_i}(\mathbf{Q}_i) + 2\mathbf{d}(\mathbf{Q}'_i) - \mathbf{d}(\mathbf{P}_i) - \mathbf{d}(\mathbf{O})\|. \quad (13)$$

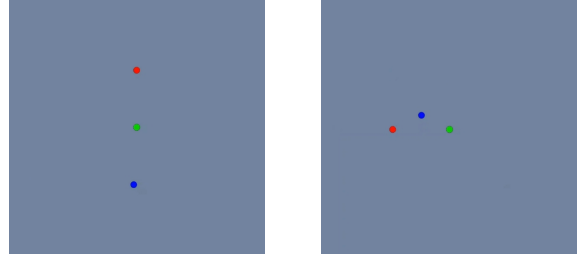
For robustness to errors in the satisfaction of the constraints, the Huber loss L_{δ} is used:

$$L_{\delta}(e) = \begin{cases} \frac{1}{2}e^2, & \text{if } |e| \leq \delta, \\ \delta(|e| - \frac{1}{2}\delta), & \text{otherwise.} \end{cases} \quad (14)$$

The parameters δ_1 and δ_2 are set to the median of the individual errors $\{e_1(\mathbf{d}, i)\}_{i=1}^{N_1}$ and $\{e_2(\mathbf{d}, i)\}_{i=1}^{N_2}$, respectively. Optimization is performed using the *patternsearch* algorithm implemented in Matlab (Audet and Dennis Jr, 2002; Kolda et al., 2006; Lewis et al., 2007).

3.4 Implementation and Practical Considerations

To ensure standardised testing conditions, participants are required to position themselves in front of the screen and rest their heads on the chin-rest to maintain a fixed distance from the screen. Being a monocular test, the participant needs to cover the fellow eye. Throughout the test, participants are required to maintain their focus on the central fixation point. As described in Section 3, there are two different central symmetrical constraints. Thus, the participant needs to displace the movable point to satisfy the constraints one by one. The test procedure is as follows:



(a) Type 1 constraint: central fixation point (green) as centre of symmetry.

(b) Type 2 constraint: blue point as centre of symmetry.

Figure 5: Screenshot showing the two different central symmetric constraints presented to the patient.

Step 1: The participant is required to manipulate the blue point to fulfil a type 1 constraint, as shown in Figure 5a. Once the participant has confirmed that the three points satisfy the constraint, they can proceed to the next randomly selected reference point.

Step 2: Repeat Step 1 until all reference points have been tested.

Step 3: The participant is required to manipulate the blue point to fulfil a type 2 constraint, as shown in Figure 5b. Once the participant has confirmed that the three points satisfy the constraint, they can proceed to the next randomly selected reference point.

Step 4: Repeat Step 3 until all reference points have been tested.

Step 5: Compute the distortion map by optimising the cost function and save the data.

This process bears some similarities with the square completion task proposed by (Wiecek et al., 2015), as both methods rely on point-based operations and employ geometric constraints. However, there are notable distinctions between the two approaches. In contrast to the square completion task, this method presents only three dots to the participant, reducing the complexity of the task. Additionally, the geometric constraints utilised by the two methods differ. While this method adopts central symmetric constraints, the square completion task primarily utilizes four corner points and four mid-points on the side to establish a regular square. In summary, when compared to the square completion task, this method offers enhanced ease of operation. Moreover, it successfully overcomes the square completion task's inherent limitation in handling asymmetrical patterns. By employing a simplified dot arrangement and a more principled set of geometric constraints, we achieve a more straightforward and accurate approach to mapping the visual distortion.

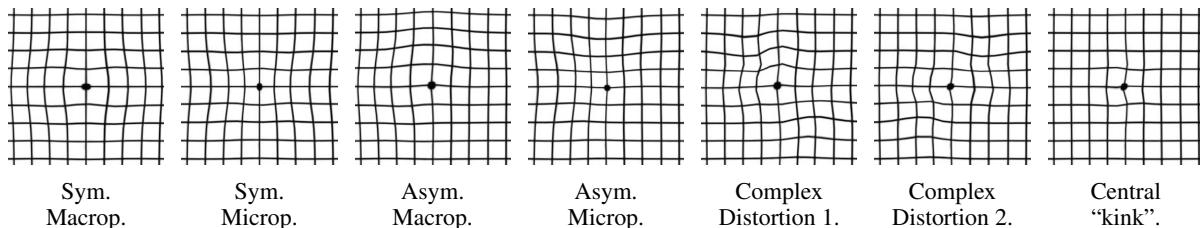


Figure 6: The seven distortion patterns used in the simulation experiments.

4 EXPERIMENTAL EVALUATION

To evaluate the approach, we conducted a series of experiments using simulated visual distortions. The evaluation considers seven different distortion patterns whose choice was informed by a discussion with an experienced ophthalmologist. The selected distortion patterns comprise symmetrical macropsia, symmetrical micropsia, asymmetrical macropsia, asymmetrical micropsia, two complex distortions, and a central “Kink” distortion, as depicted in Figure 6. Each distortion pattern provides Ground Truth (GT) information on the distortion at each pixel in the visual field and is used to calculate the correction required to enforce the central symmetry constraint for each reference point considered, thereby simulating the response of a patient.

4.1 Ablation Study

An ablation study is conducted to validate the benefit of the two types of constraints introduced. To this end, the proposed approach is evaluated using type 1 only, type 2 only and both types of constraints. Several metrics, including the structural similarity index measure (SSIM), peak signal-to-noise ratio (PSNR), and root mean square error (RMSE), are used to quantify the similarity between the mapped distortion and the GT. Since metamorphopsia primarily affects the central area of the visual field, measurements are focused on a square region centred on the central fixation point. This square has a side length equivalent to a visual angle of 10° , extending 5° outward from the central fixation point. Moreover, the number of iterations and cost function executions are also counted to measure the computational complexity.

As can be seen in Table 1, the proposed approach using both types of constraints uses far less computing power than the other approaches considering only one type of constraint while achieving comparable or better performance. Figure 7 also shows that the approach combining both types of constraints overcomes the limitation of the type 1 constraint which

Table 1: Ablation study results analysing the effect of both types of constraints on performance.

	Metric	Type 1	Type 2	Types 1 & 2
Sym. Macrop.	PSNR (dB) \uparrow	10.12	11.61	11.86
	SSIM \uparrow	0.60	0.66	0.68
	RMSE ($^\circ$) \downarrow	0.24	0.12	0.13
	Iteration \downarrow	90	158	66
	Func-Count \downarrow	1149	2028	869
Sym. Microp.	PSNR (dB) \uparrow	9.61	11.49	10.26
	SSIM \uparrow	0.57	0.66	0.60
	RMSE ($^\circ$) \downarrow	0.25	0.13	0.17
	Iteration \downarrow	264	148	108
	Func-Count \downarrow	3183	1892	1394
Asym. Macrop.	PSNR (dB) \uparrow	8.89	11.87	9.66
	SSIM \uparrow	0.52	0.72	0.57
	RMSE ($^\circ$) \downarrow	0.22	0.14	0.17
	Iteration \downarrow	174	162	118
	Func-Count \downarrow	2167	2039	1493
Asym. Microp.	PSNR (dB) \uparrow	8.25	10.19	8.55
	SSIM \uparrow	0.46	0.58	0.49
	RMSE ($^\circ$) \downarrow	0.27	0.15	0.22
	Iteration \downarrow	170	174	154
	Func-Count \downarrow	2121	2166	1867
Complex 1	PSNR (dB) \uparrow	8.93	10.39	10.90
	SSIM \uparrow	0.51	0.60	0.64
	RMSE ($^\circ$) \downarrow	0.26	0.20	0.19
	Iteration \downarrow	106	126	110
	Func-Count \downarrow	1311	1648	1364
Complex 2	PSNR (dB) \uparrow	10.114	10.329	10.326
	SSIM \uparrow	0.596	0.604	0.598
	RMSE ($^\circ$) \downarrow	0.22	0.22	0.21
	Iteration \downarrow	164	152	68
	Func-Count \downarrow	2048	1924	889
Central “kink”	PSNR (dB) \uparrow	15.82	12.59	15.37
	SSIM \uparrow	0.82	0.69	0.81
	RMSE ($^\circ$) \downarrow	0.05	0.09	0.06
	Iteration \downarrow	184	126	90
	Func-Count \downarrow	2242	1589	1141

cannot retrieve symmetric distortion patterns when used on its own. The green square denotes the specific region of interest used to calculate the metrics.

4.2 Robustness to Noise Analysis

Displacements estimated directly from the GT in order to satisfy the central symmetry constraint provide

Table 2: Experimental results for different noise levels.

Metric		No Noise	Gaussian Noise									
			5		10		15		20		25	
			Mean	Std	Mean	Std	Mean	Std	Mean	Std	Mean	Std
Sym. Macrop.	PSNR (dB) ↑	15.81	10.97	0.92	10.09	1.30	9.50	1.10	9.07	0.96	8.79	0.94
	SSIM ↑	0.82	0.64	0.05	0.59	0.07	0.55	0.07	0.52	0.07	0.49	0.07
	RMSE (°) ↓	0.07	0.15	0.03	0.19	0.05	0.24	0.08	0.29	0.10	0.34	0.11
Sym. Microp.	PSNR (dB) ↑	14.93	10.98	1.29	9.67	1.06	9.24	0.84	8.86	0.99	8.63	0.86
	SSIM ↑	0.79	0.64	0.07	0.55	0.07	0.52	0.06	0.49	0.08	0.47	0.06
	RMSE (°) ↓	0.07	0.16	0.04	0.22	0.06	0.26	0.09	0.31	0.11	0.35	0.12
Asym. Macrop.	PSNR (dB) ↑	14.44	10.10	1.11	9.85	1.19	9.36	1.10	9.04	0.88	8.78	0.89
	SSIM ↑	0.78	0.59	0.06	0.57	0.07	0.53	0.07	0.51	0.07	0.49	0.07
	RMSE (°) ↓	0.08	0.17	0.04	0.20	0.06	0.25	0.09	0.30	0.11	0.36	0.13
Asym. Microp.	PSNR (dB) ↑	12.51	9.18	1.13	9.38	1.31	9.03	1.27	8.83	0.95	8.56	0.91
	SSIM ↑	0.71	0.52	0.06	0.53	0.09	0.50	0.09	0.49	0.07	0.47	0.07
	RMSE (°) ↓	0.09	0.20	0.05	0.21	0.06	0.27	0.10	0.30	0.11	0.34	0.11
Complex 1	PSNR (dB) ↑	9.37	10.02	0.46	9.46	0.49	8.71	0.51	8.63	0.52	8.27	0.53
	SSIM ↑	0.55	0.58	0.03	0.55	0.04	0.49	0.04	0.48	0.05	0.45	0.05
	RMSE (°) ↓	0.27	0.22	0.03	0.25	0.04	0.32	0.06	0.34	0.08	0.41	0.12
Complex 2	PSNR (dB) ↑	10.46	10.06	0.57	9.48	0.62	8.80	0.59	8.60	0.63	8.38	0.56
	SSIM ↑	0.61	0.59	0.04	0.55	0.05	0.50	0.05	0.48	0.05	0.46	0.05
	RMSE (°) ↓	0.21	0.22	0.02	0.25	0.05	0.31	0.08	0.33	0.09	0.36	0.09
Central "kink"	PSNR (dB) ↑	14.87	13.05	1.33	10.91	1.56	9.76	1.31	9.20	0.84	8.72	0.91
	SSIM ↑	0.80	0.73	0.05	0.63	0.08	0.56	0.08	0.52	0.06	0.49	0.07
	RMSE (°) ↓	0.07	0.09	0.03	0.14	0.05	0.22	0.07	0.26	0.09	0.35	0.11

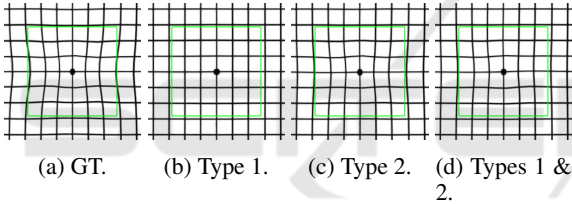


Figure 7: Example of mapped visual distortion for the symmetrical micropsia pattern using different types of constraints.

an ideal patient response that is unlikely to be possible in practice. To simulate human errors and have a more realistic evaluation scenario, random Gaussian noise is introduced to corrupt those ideal displacements. The noise is determined based on the radial visual angle distances and defined as follows for each coordinate:

$$f(x) = \frac{1}{\sqrt{2\pi}\sigma} e^{-\frac{x^2}{2\sigma^2}} \quad (15)$$

where σ represents the percentage of the radial distance to the central fixation point. This ensures that the magnitude of the added Gaussian noise is dependent on the distance from the central fixation point, to model the decrease in visual acuity the further away the point is from the fovea. To assess the robustness of the method, simulation experiments are conducted using 6 different noise levels, corresponding to σ equals to 0% (no noise), 5%, 10%, 15%, 20% and 25%, with 50 iterations for each noise level. Performance is again evaluated by comparing the mapped

distortions to the GT for each distortion pattern using the SSIM, PSNR and RMSE metrics calculated over the central region of the field of view.

Experimental results with the different noise levels are shown in Table 2. The mean and standard deviation of the 50 simulation experiments of each noise level are presented. To facilitate visual analysis of the experimental results, box and whisker plots are used, as depicted in Figure 8 in the case of the symmetrical macropsia pattern. It is evident that all three similarity measurement methods exhibit fluctuations within a certain range, attributable to the inclusion of random Gaussian noise in each experiment. As expected, it can be observed that the similarity decreases as the noise level increases.

4.3 Effect of Distortion Pattern

We now evaluate how performance is impacted by the distortion pattern. The analysis is conducted with a noise level of $\sigma = 10\%$ which was identified as most representative of the noise level seen with real patients. As can be seen in Figure 9, the symmetry completion test exhibits some robustness to noise, with nearly all PSNR values exceeding 8 dB, the majority of SSIM values surpassing 0.5 and most RMSE values falling below 0.3° . However, it is important to note that the performance in the case of complex distortion patterns is notably poorer compared to other distortion patterns. This suggests that the method exhibits limitations when confronted with complex dis-

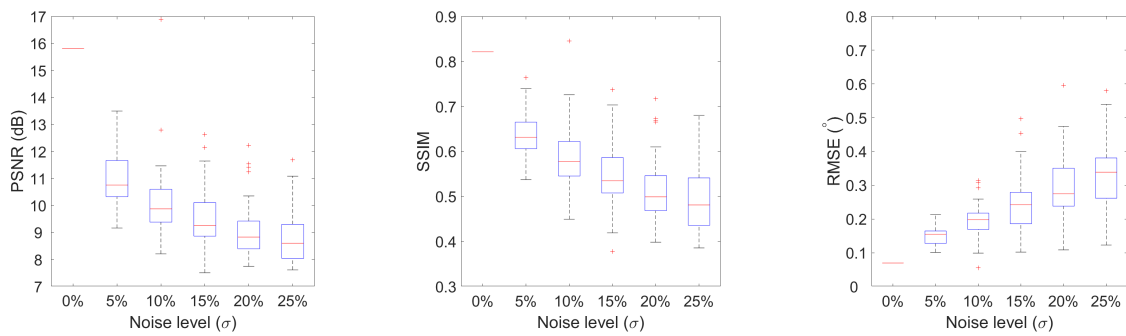


Figure 8: The different noise similarity results for the symmetrical macropsia pattern.

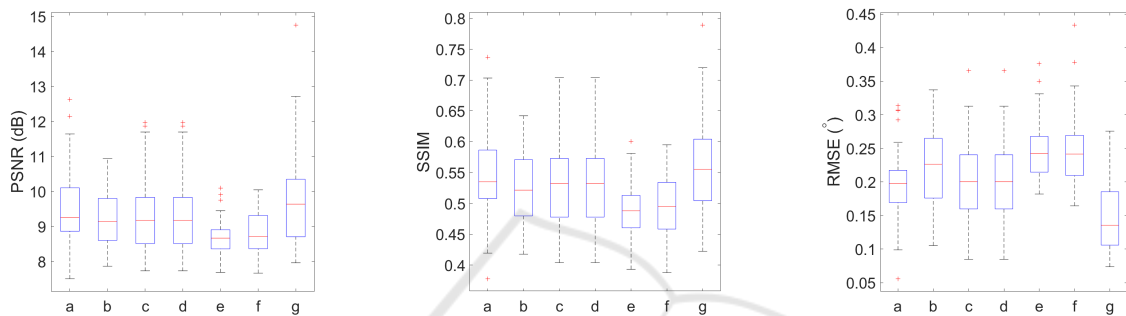


Figure 9: The seven distortion patterns similarity results of the noise level $\sigma = 10\%$. The letter labels from left to right in each figure correspond to seven distortion patterns: (a) Symmetrical macropsia; (b) Symmetrical micropsia; (c) Asymmetrical macropsia; (d) Asymmetrical micropsia; (e) Complex distortion 1; (f) Complex distortion 2; (g) Central “Kink”.

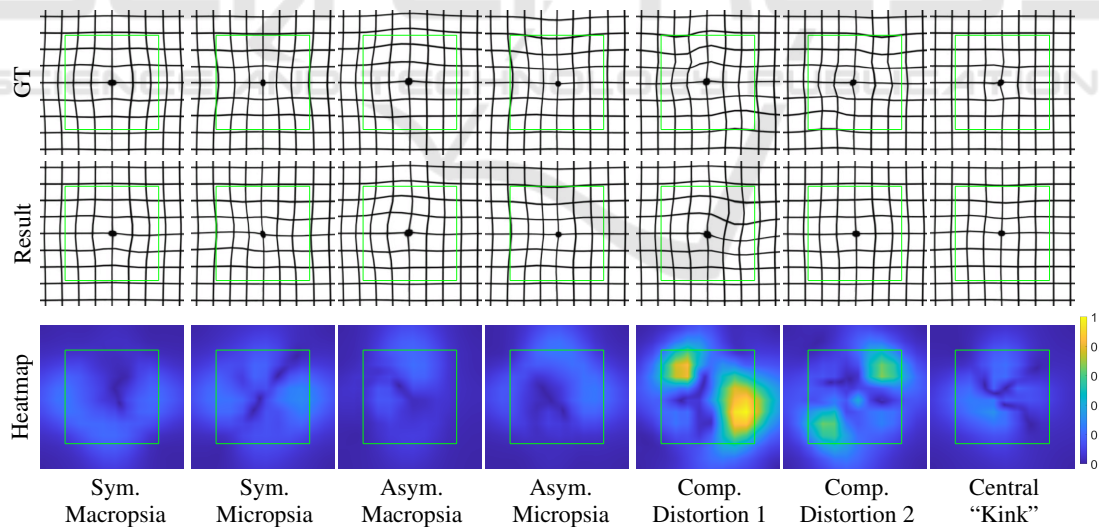


Figure 10: Estimated distortions and their error maps for some of the simulated tests in case of the seven different simulated distortion patterns for the noise level of $\sigma = 10\%$.

tortions, as the designed distortion model, which only employs four handles in the central area, struggles to adequately address such complexities.

Additionally, to visualise the disparities between the generated images and the GT, error heatmaps are computed. The heatmaps use a uniform scale across

all the results to facilitate comparison, as illustrated in Figure 10. In line with the results shown in Figure 9, the error for the complex distortion patterns exhibits more pronounced deviations compared to other patterns. In contrast, the results for symmetrical and asymmetrical patterns align closely with the GT, in-

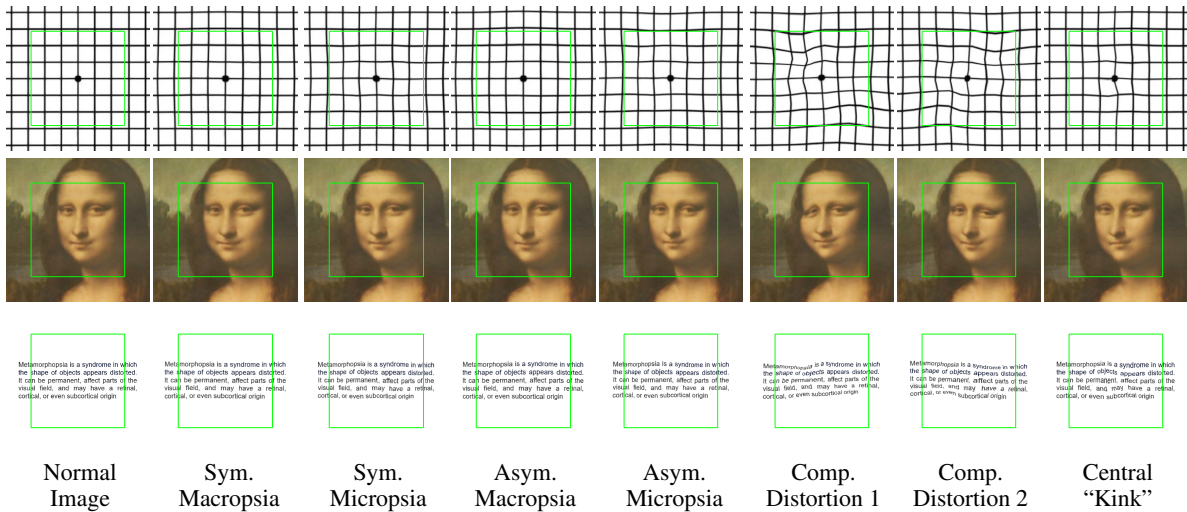


Figure 11: Correction applied on distortion results (the image should look normal if the correction is perfect) on different contents for some of the simulated tests in the case of the seven different simulated distortion patterns.

dicating the superior performance of the symmetry completion method for such distortions. As previously discussed, the method demonstrates limitations when confronted with complex distortions. Moreover, the error heatmap for the Central “Kink” pattern reveals some deviations. This can be attributed to the lack of handles at the central point of the designed MLS distortion model. This causes some difficulties in accurately mapping the distortion associated with the distortion at the central fixation point.

4.4 Correction Results

Here we assess the efficacy of the correction by comparing images that have been corrected by inverting the mapped distortion, to the original undistorted images. Different types of content are considered to illustrate the effect across different possible use cases. As illustrated in Figure 11, the symmetrical and asymmetrical distorted patterns can be corrected very effectively. For complex and central “kink” distortion patterns, the distortion has only been partially corrected with some clearly visible residual distortion.

4.5 Comparison Against Square Completion Task

As previously discussed, this method bears some similarities with the square completion task from (Wiecek et al., 2015) since both methods use points and geometric rules to operate. Therefore, a set of comparison experiments is conducted using the seven distortion patterns. The comparative evaluation is carried out in the case of the noise-free input measure-

ments. The GT distortion is used to calculate the location of the 16 points (two squares) in the square completion task. The symmetry completion test proceeds as described previously using 24 reference points. The two methods are then compared by assessing the estimated distortion at the 16 points. The 16 points representing the squares for the seven distortion patterns are displayed in Figure 12. Green represents the GT, blue shows the results of the symmetry completion test and red corresponds to the square completion task results. The symmetry completion test results are more accurate than the results of the square completion task as the blue squares are mostly perfectly aligned with the GT (the green square). Again, the symmetry completion test results for the complex distortion patterns are misaligned at the corner of the bigger square which means the distortions of these two patterns cannot be corrected perfectly. This is consistent with the previous analysis showing that this method suffers from limitations with complex distortions. Compared to the square completion task, our method successfully overcomes the square completion task’s inherent limitation in handling asymmetrical patterns, while also being able to produce a dense visual distortion map.

5 CONCLUSIONS AND FUTURE WORK

We presented a novel approach for mapping visual distortion based on low-level geometric constraints (central symmetry). We demonstrated how an energy

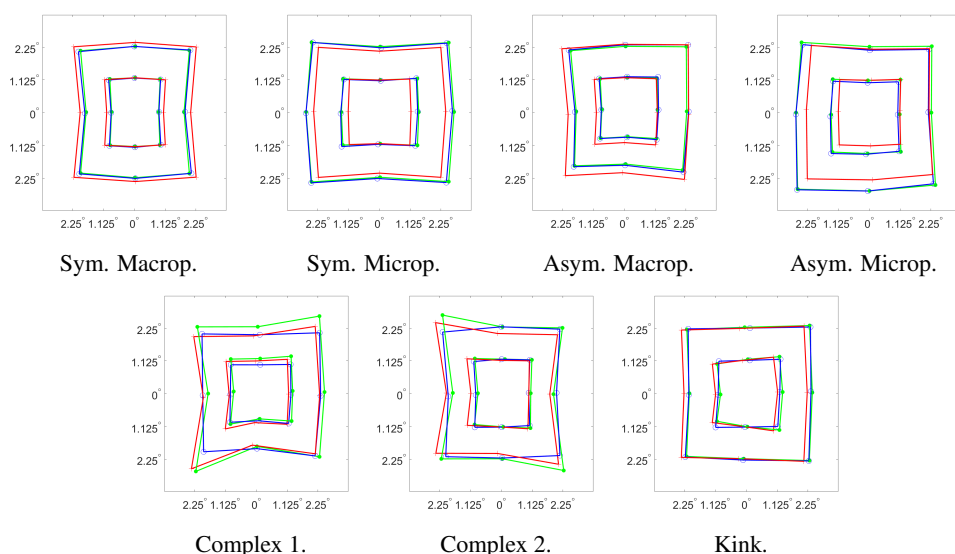


Figure 12: Comparative results for the seven distortion patterns. The green colour is the GT, the blue colour is the result of the symmetry completion test and the red colour is the result of the square completion task.

function can be defined based on these low-level constraints and effectively optimised using a parametric model of distortion based on MLS. Analysis of the simulation data reveals that the symmetry completion method is able to accurately map visual distortion and exhibits some robustness to noise. The predefined distortion model, constrained by a limited number of handles and fixed positions, suffers from inaccuracies when estimating more complex distortions. Furthermore, the absence of a handle at the central point restricts the method's ability to address distortion occurring at this location.

The demonstrated capability of this approach on simulated data to estimate visual distortion in individuals affected by metamorphopsia provides a compelling foundation for the development of an application utilizing see-through devices. The next step is to clinically evaluate the method with real patients living with metamorphopsia. The approach has received a favourable ethics opinion and is about to be clinically evaluated at St Thomas' Hospital in London with patients suffering from metamorphopsia, following the protocol outlined in (Ling et al., 2023). Moreover, as the method requires the participant to maintain the focus on the central fixation point, employing eye-tracking technology may be a good strategy to monitor the satisfaction of this constraint. Leveraging the integration of an eye tracker also holds promising potential in dynamically compensating for the distorted vision experienced by individuals with metamorphopsia. A particularly interesting avenue for future work is to investigate how the technology could benefit patients as a corrective device. In the future, we would

like to explore how these algorithms may be deployed across other types of devices such as headsets or 3D tablets and also extend the correction to dynamically adapt it to gaze direction through eye tracking.

REFERENCES

- Audet, C. and Dennis Jr, J. E. (2002). Analysis of generalized pattern searches. *SIAM Journal on Optimization*, 13(3):889–903.
- Bex, P. J. (2010). (in) sensitivity to spatial distortion in natural scenes. *Journal of Vision*, 10(2):23–23.
- Bouwens, M. D. and van Meurs, J. C. (2003). Sine ampler charts: a new method for the follow-up of metamorphopsia in patients undergoing macular pucker surgery. *Graefe's Archive for Clinical and Experimental Ophthalmology*, 241(2):89–93.
- Bozzelli, G., De Nino, M., Pero, C., and Ricciardi, S. (2020). Ar based user adaptive compensation of metamorphopsia. In *Proceedings of the International Conference on Advanced Visual Interfaces*, pages 1–5.
- Burke, W. (1999). Psychophysical observations concerned with a foveal lesion (macular hole). *Vision Research*, 39(14):2421–2427.
- Cimmino, L., Pero, C., Ricciardi, S., and Wan, S. (2021). A method for user-customized compensation of metamorphopsia through video see-through enabled head mounted display. *Pattern Recognition Letters*, 151:252–258.
- Cohen, S. Y., Lamarque, F., Saucet, J.-C., Provent, P., Langram, C., and LeGargasson, J.-F. (2003). Filling-in phenomenon in patients with age-related macular degeneration: differences regarding uni-or bilaterality of central scotoma. *Graefe's Archive for Clinical and Experimental Ophthalmology*, 241(10):785–791.

- Deemer, A. D., Bradley, C. K., Ross, N. C., Natale, D. M., Itthipanichpong, R., Werblin, F. S., and Massof, R. W. (2018). Low vision enhancement with head-mounted video display systems: are we there yet? *Optometry and Vision Science*, 95(9):694.
- Ichige, H., Toyoura, M., Go, K., Kashiwagi, K., Fujishiro, I., and Mao, X. (2019). Visual assessment of distorted view for metamorphopsia patient by interactive line manipulation. In *2019 International Conference on Cyberworlds (CW)*, pages 187–190. IEEE.
- Jensen, O. M. and Larsen, M. (1998). Objective assessment of photoreceptor displacement and metamorphopsia: a study of macular holes. *Archives of Ophthalmology*, 116(10):1303–1306.
- Kolda, T. G., Lewis, R. M., Torczon, V., et al. (2006). A generating set direct search augmented lagrangian algorithm for optimization with a combination of general and linear constraints. Technical report, Technical Report SAND2006-5315, Sandia National Laboratories.
- Lewis, R. M., Shepherd, A., and Torczon, V. (2007). Implementing generating set search methods for linearly constrained minimization. *SIAM Journal on Scientific Computing*, 29(6):2507–2530.
- Ling, Y., Frohlich, D. M., Williamson, T. H., and Guillemaut, J.-Y. (2023). A toolkit of approaches for digital mapping and correction of visual distortion. In *Proceedings of the 25th International ACM SIGACCESS Conference on Computers and Accessibility*, pages 1–5.
- Mansouri, B., Hansen, B. C., and Hess, R. F. (2009). Disrupted retinotopic maps in amblyopia. *Investigative Ophthalmology & Visual Science*, 50(7):3218–3225.
- Massof, R. W. (1998). Electro-optical head-mounted low vision enhancement. *Practical Optometry*, 9(6):214–20.
- Moritake, K., Zhu, Z., Toyoura, M., Go, K., Kashiwagi, K., Fujishiro, I., and Mao, X. (2021). Eye-tracker-free compensation for metamorphopsia. In *2021 International Conference on Cyberworlds (CW)*, pages 78–84. IEEE.
- Ong, J., Zaman, N., Waisberg, E., Kamran, S. A., Lee, A. G., and Tavakkoli, A. (2022). Head-mounted digital metamorphopsia suppression as a countermeasure for macular-related visual distortions for prolonged spaceflight missions and terrestrial health. *Wearable Technologies*, 3:e26.
- Peli, E. (1994). Binary head-mounted display as a low vision aid: 1: 40 pm (lv-109). *Optometry and Vision Science*, 71(12):21.
- Peli, E. and Peli, T. (1984). Image enhancement for the visually impaired. *Optical Engineering*, 23(1):47–51.
- Schaefer, S., McPhail, T., and Warren, J. (2006). Image deformation using moving least squares. In *ACM SIGGRAPH 2006 Papers*, pages 533–540.
- Simunovic, M. P. (2015). Metamorphopsia and its quantification. *Retina*, 35(7):1285–1291.
- Szpiro, S. F. A., Hashash, S., Zhao, Y., and Azenkot, S. (2016). How people with low vision access computing devices: Understanding challenges and opportunities. In *Proceedings of the 18th International ACM SIGACCESS Conference on Computers and Accessibility*, pages 171–180.
- Ugarte, M., Shunmugam, M., Laidlaw, D. A. H., and Williamson, T. H. (2013). Morphision: a method for subjective evaluation of metamorphopsia in patients with unilateral macular pathology (ie, full thickness macular hole and epiretinal membrane). *Indian Journal of Ophthalmology*, 61(11):653.
- Vargas-Martín, F., Peláez-Coca, M. D., Ros, E., Diaz, J., and Mota, S. (2005). A generic real-time video processing unit for low vision. In *International Congress Series*, volume 1282, pages 1075–1079. Elsevier.
- WHO-Newsroom (2023). Blindness and vision impairment.
- Wiecek, E., Lashkari, K., Dakin, S. C., and Bex, P. (2015). Novel quantitative assessment of metamorphopsia in maculopathy. *Investigative Ophthalmology & Visual Science*, 56(1):494–504.
- Zaman, N., Tavakkoli, A., and Zuckerbrod, S. (2020). A mixed reality system for modeling perceptual deficit to correct neural errors and recover functional vision. In *2020 IEEE Conference on Virtual Reality and 3D User Interfaces Abstracts and Workshops (VRW)*, pages 269–274. IEEE.
- Zhao, Y., Szpiro, S., Shi, L., and Azenkot, S. (2019). Designing and evaluating a customizable head-mounted vision enhancement system for people with low vision. *ACM Transactions on Accessible Computing (TACCESS)*, 12(4):1–46.
- Zhu, Z., Toyoura, M., Fujishiro, I., Go, K., Kashiwagi, K., and Mao, X. (2022). Linem: assessing metamorphopsia symptom using line manipulation task. *The Visual Computer*, 38(5):1607–1617.
- Zur, D. and Ullman, S. (2003). Filling-in of retinal scotomas. *Vision Research*, 43(9):971–982.